Strong Doping of the *n*-Optical Confinement Layer for Increasing Output Power of High-Power Pulsed Laser Diodes in the Eye Safe Wavelength Range

Boris S. Ryvkin[1,2], Eugene A.Avrutin[3], and Juha T.Kostamovaara[1]

[1] Dept of Electrical and Information Engineering, University of Oulu, Oulu, Finland
[2]A F Ioffe Physico-Technical Institute, St.Petersburg, Russia
[3] Dept of Electronics, University of York, York, UK; corresponding author

E-mail: eugene.avrutin@york.ac.uk

Abstract—An analytical model for internal optical losses at high power in a 1.5 μm laser diode with strong *n*-doping in the *n*-side of the optical confinement layer is created. The model includes intervalence band absorption by holes supplied by both current flow and two-photon absorption, as well as the direct two-photon absorption effect. The resulting losses are compared with those in an identical structure with a weakly doped waveguide, and shown to be substantially lower, resulting in a significant improvement in the output power and efficiency in the structure with a strongly doped waveguide.

***Index Terms*— high power lasers, laser efficiency, laser theory, semiconductor lasers**

1. Introduction.

High-power pulsed diode lasers operating in the eye-safe region of 1400-1700 nm are becoming increasingly important, for applications ranging from EDFA pumping to laser radar technology.

However obtaining high output power within this spectral range is a more complex task than for shorter wavelengths of ~ 1 μm (see, for a recent example, experimental dependences 2 on Figures 2 and 4 in[1]), owing mainly to higher optical losses at high currents in InGaAsP and AlGaInAs quaternary compound materials capable of laser emission in the eye safe range.

The origin of this effect is to a significant degree in the accumulation of carriers in the OCL at high currents (see e.g. [2] and references therein). The effect on this carrier accumulation on optical losses is particularly strong in the InGaAsP and AlGaInAs quaternaries, for at least two reasons. Firstly, in quaternary III-V materials in the eye safe spectral region, the free-hole Intervalence Band Absorption (IVBA) cross-section, which scales the optical losses, is rather high (2-6×10^{-17} cm^2 [3], [4], as opposed to ~1×10^{-17} cm^2 typical for GaAs/AlGaAs materials at ~ 1 μm). Crucially, the ratio of the IVBA (free hole) cross section to the free electron absorption cross-section, which is greater than one in all III-V materials, is particularly high (almost two orders of magnitude) in the quaternary materials [4] [5]: for the free electron absorption cross section, a range of $(0.1\text{-}1)\times10^{-18}$ cm^2 has been quoted [5]. Secondly, the low hole diffusion coefficients in the OCL can lead to a high density of inhomogeneously distributed nonequilibrium carriers (both electrons and holes) in the OCL, which has its origin in the carrier transport through the OCL and in the carrier generation by two-photon absorption and leads to optical and recombination losses as discussed in [2, 6].

In [7], we developed an analytical theory for the inhomogeneous carrier accumulation in a weakly doped Optical Confinement Layer due to the current flow and its influence on the optical losses, showing that that mechanism was the dominant one in broadened laser structures with a (near-) symmetric position of the active layer (AL) such as the one realised in Refs. [1, 8]. The theory, which has since been confirmed by both numerical simulations [9] [10] and experimental indications [9] [11], shows that, due to the diffusion of the holes being much weaker than that of the electrons, the inhomogeneous carrier accumulation at the *p*-side of the OCL, between the AL and the *p*-cladding, is considerably stronger than that at the *n*-side, between the *n*-cladding and the AL. Later, the theory was extended to the case of doped OCL [12]. The calculations based on this model show that, although *p*-doping of the *p*-side of the OCL reduces the build-up of nonequilibrium carriers caused by the current flow, the effect of this on internal loss is, under all conditions and in all designs studied, not as strong as the absorption by equilibrium holes introduced by the doping itself. The net effect of *p*-doping on

the optical properties of the laser is thus always an increase in the optical losses. At moderate currents, the effect of this on the wall-plug efficiency can be overcome by the decrease in the electrical resistance with doping; however at high currents, the latter effect was shown [12] to be rather weak.

This dictates a strategy in counteracting the effect of the current-induced carrier accumulation on the optical losses at high power, namely using some type of a laser design with an asymmetric position of the AL, much closer to the *p*-cladding than to the n-cladding , ensuring that the *p*-OCL is thin, in the extreme asymmetry case almost non-existent. In a version of this design used by a number of teams (including ourselves) [13-17], the asymmetric AL position is combined with the asymmetry of the refractive index steps at the interfaces of the OCL with the *n*-cladding (small step) and *p*-cladding (large step), which is termed Extreme Double Asymmetric design [14]. Such lasers allow single transverse mode operation in arbitrarily broad lasers and have indeed demonstrated high power pulsed operation (at λ~1μm) in broad-area designs.

Another design with the AL near *p*-cladding is that of the Slab Coupled Optical Waveguide devices, including lasers (SCOWL) and Amplifiers; see e.g. [18] and references therein), which can have even lower built-in losses and has been used successfully for high-power generation (at λ~1μm) in CW and mode-locked regimes, albeit from relatively narrow stripes (in broad area lasers, this design does not necessarily guarantee single transverse mode operation).

However even lasers with an asymmetric AL position and waveguide (operating at λ~1μm) still exhibit saturation of optical power at high injection level [14] indicating the presence of some optical losses increasing with current. At least two mechanisms can contribute to this. The first is the inhomogeneous current-induced accumulation of carriers (of both signs simultaneously) in the *n*-OCL, which, although weaker than the effect in the *p*-OCL, may become of some importance if the *n*-OCL is very broad (a few micrometres, as in SCOWLs for example) and the IVBA cross-section is high. The second mechanism is related to the effects of Two-Photon-Absorption (TPA), both direct and indirect, the latter being due to Free Carrier Absorption (FCA) by TPA-generated carriers in the OCL, most importantly IVBA by TPA-generated holes [19] [2],[6]. As shown in our recent analysis [2, 6], the indirect effect becomes important in waveguides with an asymmetric AL location, in which the AL (the drain location for TPA-excited carriers) is far from the mode peak (where the maximum of carrier generation is located).

Here, we show that in lasers operating in the eye safe spectral range, the effects of IVBA by nonequilibrium carriers can be substantially weakened by strong *n*-doping of the *n*-OCL. Such doping effectively removes both the carriers accumulated due to the transport (in the doped material, the *drift* current dominates [12], making for fast carrier transport towards the AL) and those generated by the TPA (mainly by introducing additional carrier dissipation through recombination). This is to some extent counteracted by some carriers being supplied by the doping itself. However, inhomogeneously distributed carriers whose density is reduced by doping are both electrons and holes in equal quantities, whereas *only electrons* are introduced by *n*-doping. Since the free-hole absorption cross section in InGaAsP quaternaries is much greater than the free-electron absorption cross section, the net effect, unlike the case of *p*-doping, is a pronounced reduction of loss. This effect will be quantified and analysed below.

2. Analysis and Results.

A. The Structure Analysed

The InGaAsP structure, designed to emit at λ≈1.5 μm, is shown in Fig. 1. The bulk InGaAsP AL, with the composition as in [20], is located just ~0.15 μm (which is thus the thickness of the *p*-OCL) from the *p*-cladding; the *p*-OCL is assumed to be relatively highly doped (say 5×10^{17} cm^{-3}); a similar doping level is assumed at the adjacent part of the *p*-cladding itself. This does not cause a strong optical loss due to the small thickness of the p-OCL and weak penetration of the mode into the *p*-cladding. Despite the broad total width of the OCL (h=3 μm), the small refractive index step at the *n*-OCL/ *n*-cladding interface ensures that the waveguide supports a single transverse mode, whose profile is also shown. The calculated fast-axis far field width is about 17 degrees FWHM.

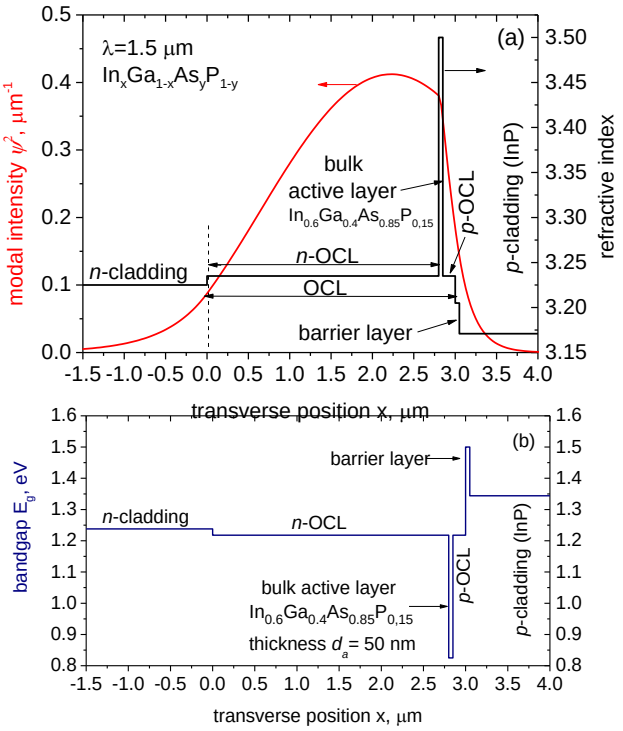

Fig. 1. (a) Schematic of the waveguide structure evaluated and the corresponding intensity distributions in the (fundamental) transverse waveguide mode; (b) the bandgap profile of the waveguide

The doping of the broad *n*-OCL is not fixed and is the main subject of this paper. Below, it will be shown that the lowest OCL optical losses at high injection levels can be realised in the case of highly doped (with the ionised donor density N_D>10^{18}cm^{-3}) *n*-OCL; however, the opposite case of very low OCL doping (N_D~10^{16}cm^{-3}) will be presented for comparison and reference.

B. *Carrier Accumulation In The Optical Confinement Layer At High Injection Levels*

Following the previous work [6], we shall use the fact that as long as the carrier densities in the OCL remain moderate enough for the nonlinear recombination to remain negligible, as is the case in this study, the transport problem in the OCL is a *linear* one as regards the nonequilibrium carrier density for both high and low doping. This allows us to separate the nonequilibrium carrier density profile in the (*n*-) OCL $\Delta N(x) = N_h(x) = N_e(x) - N_D$ (N_e and N_h being electron and hole densities) into three parts:

$$\Delta N(x) = N_b + \Delta N_j(x) + \Delta N_{TPA}(x) \qquad (1)$$

The first term, N_b , in Eq. (1) is the spatially homogeneous background due to the nonzero time of carrier capture and the finite time of escape, which can be estimated (see [6] and references therein) as:

$$N_b \approx \frac{j}{ed_a}\tau_{cap} + N_{bT} \qquad (2)$$

where τ_{cap} is the characteristic time of carrier capture into the AL, which can be expected to be very short (subpicosecond) in our bulk active layer; we used τ_{cap} = 0.1 ps=*const*. The term N_{bT} describes the thermal escape from the AL into the OCL. This value is determined by the laser parameters and the separation between the quasi Fermi levels of electrons and holes in the AL, which were obtained simultaneously with calculating the current-dependent effective threshold, see Eq. (10) below. Under room temperature operation (which is the subject of this paper, which considers an operation regime under pulsed pumping with the usual pumping pulse duration of ~ 10-100 ns, so the laser operates in steady state, but the heating can be neglected) it does not exceed ~10^{16} cm^{-3} in the structure considered.

We shall consider next the inhomogeneous nonequilibrium carrier accumulation due to the injection current flow $\Delta N_j(x)$.

To the best of our knowledge, the *n*-OCL in high-power pulsed laser diodes and semiconductor optical amplifiers is usually undoped or relatively weakly doped (up to the ionised donor density of N_D<10^{17} cm^{-3}) [8, 9, 15, 18]. In such a case, under high injection level, the current mechanism in the *n*-OCL is almost entirely ambipolar diffusion. As shown in [7], this corresponds to the carrier (electron and hole) density accumulated in the *n*-OCL due to the current flow increasing linearly from the AL to the *n*-cladding interface $\Delta N_j(x) \approx \frac{j}{2eD_e}(l_a - x)$ (Fig. 2, the dashed curve):, where *j* is the current density, D_e, the electron diffusion coefficient (we used the value from [21]; see Table 1), and l_a, the *n*-OCL/AL interface position.

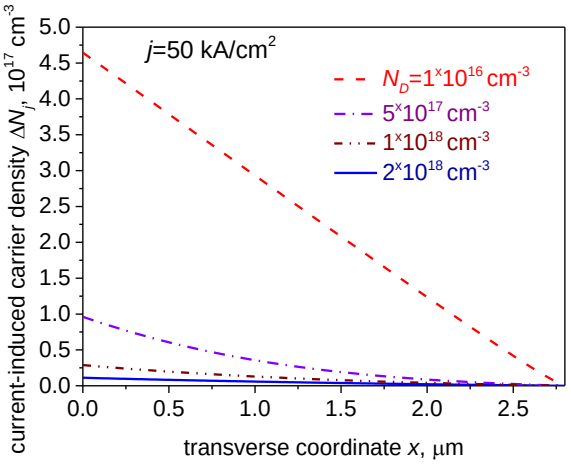

Fig. 2. Transverse profile of the current-induced nonequilibrium carrier density ΔN_j at a given current density (j=50 kA/cm^2) for different *n*-OCL doping levels.

As the doping increases, the drift component of the current becomes increasingly important, and at N_D>5×10^{17} cm^{-3}, the current is almost entirely due to drift. The distribution $\Delta N_j(x)$ for this case can be calculated following the approach of [12]; neglecting recombination, this results in a relatively simple transcendental equation (Eq.(9) in [12]). With the materials of Fig. 1, the calculated value of $\Delta N_j(x)$ does not exceed ~5×10^{16} cm^2<<N_D (as shown in Fig. 2, the solid curve).

The contributions of free-carrier absorption by the current-induced and thermally-excited carriers to to the internal loss can then be calculated as in [6]:

$$\alpha_j^{(FC)} \approx (\sigma_e + \sigma_h)\int_0^{l_a}\left[N_b - N_{bT} + \Delta N_j(x)\right]\psi^2(x)dx \qquad (3a)$$

$$\alpha_T^{(FC)}(i) = (\sigma_e + \sigma_h)\left(\Gamma_{n-OCL} + \Gamma_{p-OCL}\right)N_{bT} \qquad (3b)$$

Here, $\psi(x)$ is the amplitude profile of the transverse mode of the laser waveguide, normalised so that $\int_{-\infty}^{\infty}\psi^2(x)dx = 1$; see Appendix for more detail.

Fig. 3 shows the dependence of $\alpha_j^{(FC)}$ on doping for several current density values, assuming negligible ΔN_{TPA} for the time being. For the free-carrier absorption cross-sections, we used σ_e~0.05×10^{-17} cm^2 [4, 5] , σ_h~4×10^{-17} cm^2 [3], both of which are approximately in the middle of the range of values quoted in the literature.

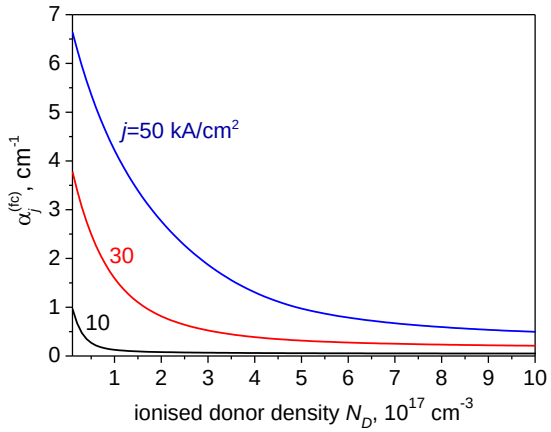

Fig.3. *n*-OCL doping level dependence of the internal absorption due to current-induced nonequilibrium carriers at different currents.

As can be seen in the figure, the doping significantly reduces the absorption even at highest current densities. The value of N_D~3×10^{17} cm^{-3} is sufficient to reduce the absorption significantly; further doping does not offer any appreciable advantage in reducing absorption due to this mechanism.

We turn next to the carrier accumulation due to Two-Photon absorption (TPA) in the OCL, which is represented by the third term $\Delta N_{TPA}(x)$ in Eq. (1), proportional to the square of the optical power.

For the case of low-doped OCL, this effect was considered theoretically in our previous paper [6], with calculations performed for the case of GaAs/AlGaAs lasers working at λ≈1 μm. In that case, the carrier density was entirely determined by their ambipolar diffusion towards, and subsequent capture into, the AL. This can potentially lead to a substantial hole (and electron) density in the OCL, which, just as the current-induced carrier accumulation, increases the losses via IVBA. We note that InGaAsP quaternaries operating at λ≈1.5 μm, in addition to having slower hole diffusion (we used the values from [21]) and higher IVBA cross-section than GaAs/AlGaAs materials, also have a higher TPA coefficient (β_2≈6×10^{-8} cm/W [19]), which makes the effect of TPA-generated carriers potentially rather detrimental. However, we argue that this effect, like the current induced loss, can be reduced by *n*-doping the *n*-OCL. For this absorption reduction to be effective, the level of doping should be such that the recombination time of nonequilibrium minority holes is comparable to, or smaller than, the characteristic time of transport of those holes towards the AL. This corresponds to the highly doped case, $N_D>>\Delta N_{TPA}$, ΔN_{TPA} being the density of nonequilibrium carriers due to TPA (equal for electrons and holes). In this case, current continuity equations give a single differential equation for the hole density ΔN_{TPA} within the *n*-OCL ($0<x<l_a$,) in the form (see, for example, [22]):

$$D_h \frac{d^2\Delta N_{TPA}}{dx^2} - v_h \frac{d\Delta N_{TPA}}{dx} - \frac{\Delta N_{TPA}}{\tau} + G(x) = 0 \qquad (4)$$

Here, D_h is the minority hole diffusion coefficient; $v_h = \mu_h E$ (μ_h being the hole mobility) is the hole drift velocity in the electric field $E = j/(e\mu_e N_D)$, j being the current density and μ_e the majority electron mobility. Thus, $v_h = (\mu_h/\mu_e)\, j/(eN_D)$; in this form it is clear that the expression contains a small parameter μ_h/μ_e and so under all realistic conditions we can assume that the second term in (4) is negligible, which substantially simplifies the calculations. Furthermore, $\tau = \left(\frac{1}{\tau_{NR}^{OCL}} + B_{OCL} N_D + C_{OCL} N_D^2 \right)^{-1}$ is the carrier lifetime in the *n*-OCL, taking into account the nonradiative recombination with a time τ_{NR}^{OCL} ~100 ns, spontaneous and Auger recombination with coefficients B_{OCL} and C_{OCL}, respectively. Note that the fact that this time is approximately constant (which in its turn is ensured by the condition $N_D>>\Delta N_{TPA},\Delta N_j$) is what allows us to consider ΔN_{TPA} and ΔN_j as two distinct populations which can be treated additively.

Finally, the TPA-related generation term $G(x)$, as in the case of the low-doped OCL treated in [6], is given by

$$G(x) = \frac{\beta_2^{(OCL)}}{\hbar\omega}\left(\frac{P}{w}\right)^2 \psi^4(x) \qquad (5)$$

Here, $\beta_2^{(OCL)}$ is the TPA coefficient in the OCL, P is the intracavity lasing power (for simplicity, we shall consider a longitudinally lumped model here), w is the stripe width.

The boundary condition to Eq. (4) at the *n*-OCL/AL interface is

$$\Delta N_{TPA}\big|_{x=l_a-} \approx 0 \qquad (6)$$

(strictly speaking, there is a nonzero boundary value, determined by the nonzero time of capture of *TPA-generated* carriers from the OCL into the AL and the finite time of thermal escape in the opposite direction, but estimates show that this value is negligible).

The boundary conditions at the opposite, *n*-cladding/OCL, interface in general, need to, firstly, ensure the continuity of minority carrier flux and, secondly, reflect a potential barrier for holes at the interface. In this paper, we restrict ourselves to the case of a waveguide broad enough to ensure that the mode intensity, and hence the generation term in the cladding is weak. Then, the hole flux from the cladding to the waveguide is negligible. At the same time, the barrier for holes is assumed to be high enough to eliminate their flux from the waveguide to the cladding (which can be achieved, for example, by strongly doping the *n*-cladding compared to the *n*-OCL). Then, there is no need to consider the nonequilibrium carrier density in the *n*-cladding, and the approximate boundary condition, which we shall use in this work, is written simply as

$$D_h \frac{d\Delta N_{TPA}}{dx}\bigg|_{x=0+} = 0 \qquad (7)$$

The solution of Eq.(4) with boundary conditions (6)- (7) is relatively straightforward; the explicit expressions are shown in

the Appendix. The simulation parameters used are summarized in Table 1.

TABLE 1. The main parameters in the calculations.

Parameter and notation		Value	Units	from
electron diffusion coefficient, N_D =10^{16} to 2×10^{18} cm^{-3}	D_e	90 to 40	cm^2/s	[21]
hole diffusion coefficient, N_D~10^{16} cm^{-3}	D_h	2.2		
hole diffusion coefficient, N_D=2×10^{18} cm^{-3}	D_h	1.3		
free electron absorption cross-section	σ_e	5×10^{-19}	cm^2	[4, 5]
IVBA cross-section	σ_h	4×10^{-17}	cm^2	[3]
TPA coefficient	β_2	6×10^{-8}	cm/W	[19]
Bimolecular recombination coefficient	B	1×10^{-10}	cm^3/s	[3]
Auger recombination coefficient, OCL	C_{OCL}	1×10^{-29}	cm^6/s	[3]
Auger recombination coefficient, active layer	C	8×10^{-29}	cm^6/s	[25]
transparency carrier density	N_{tr}	6.5×10^{17}	cm^{-3}	[20]
gain cross-section	σ_g	3.1×10^{-16}	cm^2	[20]
cavity length	L	2	mm	
stripe width	w	100	μm	
AR coating reflectance	R_{AR}	0.05		
HR coating reflectance	R_{HR}	0.95		
active layer thickness	d_a	50	nm	

Fig. 4 shows the calculated distributions of TPA-generated nonequilibrium holes (and electrons) in the *n*-OCL for a given optical power inside the resonator and either low, or very high, doping (for the low-doped case, as in [6], the carrier transport and distribution are determined by the ambipolar diffusion, so the diffusion coefficient $D_a \approx 2D_h$ was used in calculations). A substantial reduction in ΔN_{TPA} in the entire *n*-waveguide is seen, including at or near the peak of the transverse mode intensity distribution. Note that the same power corresponds to different currents in the case of different dopings; the carrier distirbutions at the same current will be shown below.

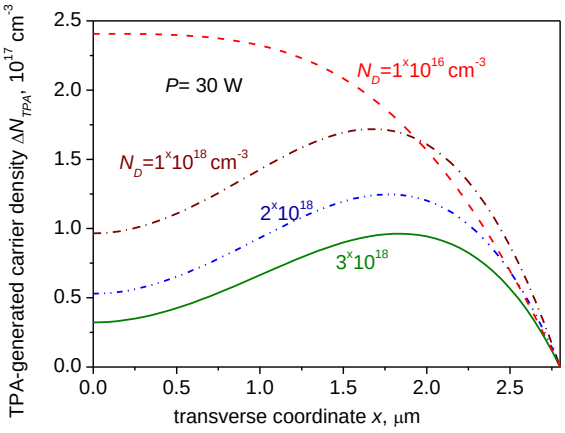

Fig.4. Transverse profile of the TPA-induced nonequilibrium carrier density ΔN_{TPA} at a given light power (P=30 W) for different *n*-OCL doping levels

The absorption due to ΔN_{TPA} is evaluated as in [6]:

$$\alpha_{TPA}^{(FC)} \approx (\sigma_e + \sigma_h) \int_0^{l_a} \Delta N_{TPA}(x,z)\psi^2(x)dx \qquad (8)$$

The results are shown in Fig. 5 as function of output power, for low and high *n*-doping levels. As as in the case of $\alpha_{TPA}^{(j)}$, a pronounced reduction of absorption by doping is seen. In the case of TPA-generated carriers, however, it is the recombination rather than the drift transport that mainly depletes the carrier accumulation and hence reduces the absorption.

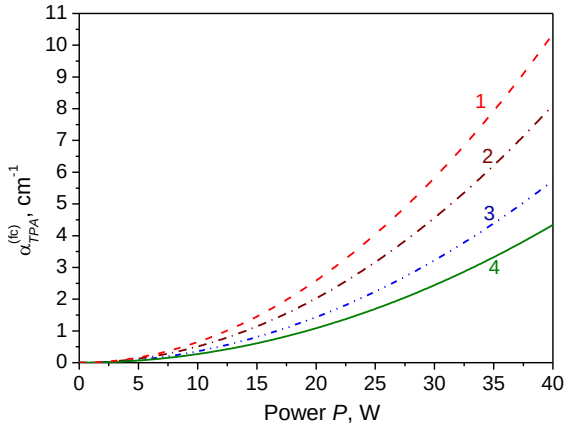

Fig.5. Power dependence of the internal absorption due to TPA-induced nonequilibrium carriers for the doping levels in the *n*-OCL of 1×10^{16} cm^{-3} (1), 1×10^{18} cm^{-3} (2), 2×10^{18} cm^{-3} (3), 3×10^{18} cm^{-3} (4).

The effect of OCL carrier recombination on injection efficiency is assumed to be weak, firstly, because of the relatively modest carrier densities in the *n*-OCL (see e.g. Fig. 2), and, secondly, because the carrier recombination in the *n*-OCL is largely balanced by the generation of carriers by TPA. Hence the injection efficiency can be assumed to be approximately unity. Then, we can calculate the output power using a transcendental equation

$$P(i) = \frac{\hbar\omega}{e}\frac{\alpha_{out}}{\alpha_{out} + \alpha_{in}(i,P(i))}(i - i_{th}(i)) \qquad (9)$$

where the output loss $\alpha_{out} = \frac{1}{2L}\ln\frac{1}{R_{HR}R_{AR}}$ was calculated assuming the high-reflectance and antireflection coated facet reflectances R_{HR}=0.95, R_{AR}=0.05, and the increase in the effective threshold current value $i_{th}(i)$ with current due to the increased α_{in} was taken into account in the calculations simultaneously with calculating the current and power-dependent losses as described below.

The internal loss was, as in [6], calculated as a sum of all contributions

$$\alpha_{in}(i,P(i)) \approx \alpha_{in}^{(\text{built-in})} + \alpha_j^{(FC)}(i) + \alpha_T^{(FC)}(i) + \alpha_{TPA}^{(FC)}(P(i)) + \alpha_{TPA}^{(\text{mod})}(P(i)) + \alpha_{AL}^{(FC)}(i) \qquad (10)$$

The first term in (10), the constant built-in absorption $\alpha_{in}^{(\text{built-in})}$, had to include the effects of both cladding and OCL doping, as well as the contribution of the structure imperfections $\alpha_{in}^{(imperf)}$:

$$\begin{aligned}\alpha_{in}^{(\text{built-in})} &= \sigma_e\left(\Gamma_{n-cl}N_D^{n-cl} + \Gamma_{n-OCL}N_D\right)\\ &+\sigma_h\left(\Gamma_{p-cl}N_A^{p-cl} + \Gamma_{p-OCL}N_A^{p-OCL}\right) + \alpha_{in}^{(imperf)}\end{aligned} \tag{11}$$

Note that, despite the mode overlap with *n*-OCL Γ_{n-OCL} being larger than its *p*-side counterpart Γ_{p-OCL}, the condition $\sigma_h >> \sigma_e$ means that it is the *p*-side of the waveguide (*p*-OCL, barrier layer, and *p*-cladding) that contributes the most to the built-in loss, despite having a total overlap with the mode of just ≈0.07. Assuming the imperfections contribution of 0.5 cm^{-1}, the total built-in absorption was calculated to vary linearly with the *n*-OCL doping level from 2.0 cm^{-1} at $N_D = 10^{16}$ cm^{-3} to 2.9 cm^{-1} at 2×10^{18} cm^{-3}, given the overlap of $\Gamma_{n-cl} + \Gamma_{n-OCL} \approx 0.9$. In the *p*-OCL and the part of the *p*-cladding adjacent to it, *p*-doping to $N_A = 5\times10^{17}$ cm^{-3} was assumed.

Furthermore, the terms $\alpha_j^{(FC)}$ and $\alpha_T^{(FC)}$ in (10) are given by Eq. (3a) and (3b). The thermal background hole density N_{bT} which determines $\alpha_T^{(FC)}$ via (3b), was evaluated from $N_{th}(i)$. In the case of a weakly doped *n*-OCL, this was done using the formula of [23], and in the case of a strongly doped OCL, using the activation formula similar to that of [24]:

$$N_{bT} = N_c^{OCL}\exp(-\left(E_g^{OCL} - \Delta E_F^{act} + \delta E_{Fe}^{n-OCL}\right)/k_BT),$$

in which N_c^{OCL} and E_g^{OCL} stand, respectively, for the equivalent electron density of states and the bandgap of the OCL, ΔE_F^{act} is the quasi Fermi level separation in the active layer calculated from $N_{th}(i)$, and δE_{Fe}^{n-OCL} is the electron quasi Fermi level in the *n*-OCL measured from the band edge. Estimates showed that, in our room-temperature case, the value of N_{bT} was very small (~10^{16} cm^{-3}) in the low doping case and negligible in the high doping case; however the situation can be expected to be different in a true CW regime with associated heating.

As regards TPA related contributions in (10), the effect of FVA by TPA-created carriers $\alpha_{TPA}^{(FC)}$ was given by (8), whereas he direct contribution $\alpha_{TPA}^{(\text{mod})}$ of the TPA to the modal losses was calculated in the same way as in [6]:

$$\alpha_{TPA}^{(\text{mod})} \approx \left(\frac{\beta_2^{(OCL)}}{w}\int_{-\infty}^{\infty}\psi^4(x)dx\right)$$

The final term in (10) represents the FCA by carriers in the actie layer,

$$\alpha_{AL}^{(\text{FC})}(i) = \left(\sigma_e^{(a)} + \sigma_h^{(a)}\right)\Gamma_a N_{th}(i) \tag{12}$$

, where Γ_a is the active layer confinement factor, $\sigma_{e,h}^{(a)}$ are the FCA cross-sections in the AL, and $N_{th}(i)$ is the current-dependent threshold carrier density. For the gain-carrier density relationship, we use the linear approximation

$$g(N) = \sigma_g(N - N_{tr}) \tag{13}$$

quite often used for bulk materials and validated [20] by the fitting the dependence to experimental data; the gain cross-section σ_g and the transparency carrier density N_{tr} were taken from that paper and are shown in Table 1.

The active layer carrier density $N_{th}(i)$ can then, using the linear nature of both relations (12) and (13), be evaluated simply as

$$N_{th}(i) = \frac{\alpha'_{in}(i,P) + \alpha_{out}}{\Gamma_a\left[\sigma_g - \left(\sigma_e^{(a)} + \sigma_h^{(a)}\right)\right]} + N_{tr} \tag{14}$$

Where $\alpha'_{in}(i,P) = \alpha_{in}(i,P) - \alpha_{AL}^{(\text{FC})}(i)$ is the sum of all contributions in (10) except $\alpha_{AL}^{(\text{FC})}(i)$. The current-dependent threshold current is then evaluated as

$$i_{th}(i) = ed_a wL\left(N/\tau_{nr} + BN_{th}^2(i) + CN_{th}^3(i)\right) \tag{15}$$

The Auger recombination coefficient *C* was taken from [25], the spontaneous recombination coefficient *B*, from [3], and the nonradiative linear recombination was taken as very weak (τ_{nr}~100 ns as in the OCL) assuming good material quality. The iterative solution of (9) and (14)-(15) then allows the light-current curve (Figure 6) to be calculated. Note that, in general, Eq. (14) is itself transcendental. In the highly doped OCL case, the negligible magnitude of the thermally escaped carrier density and the associated losses $\alpha_T^{(FC)}$ means that the right-hand-side of (14) does not explicitly depend on $N_{th.}$, so for given *i* and *P* at each step of the iterative solution, (14) is effectively a closed-form equation, which simplifies the numerical procedure. In the case of low OCL doping, 1-2 direct iterations were enough to take into account $\alpha_T^{(FC)}$.

Note also that the use of the lumped equation (9) implies the neglect of Longitudinal Spatial Hole Burning. In the structures analysed, with a relatively high AR coated facet reflectance of 0.05 and the relatively short length of 2 mm, its effect can indeed be expected to be quite weak; it becomes important for longer samples and lower AR coating [10].

The calculated power vs current curves are shown in Fig. 6 for the case of both lightly and strongly doped *n*-waveguide. The advantage of the doped structure is clear. The origin of this predicted advantage is mainly the reduction in the current-induced carrier density, but the reduction in the TPA-induced carrier accumulation plays a part as well.

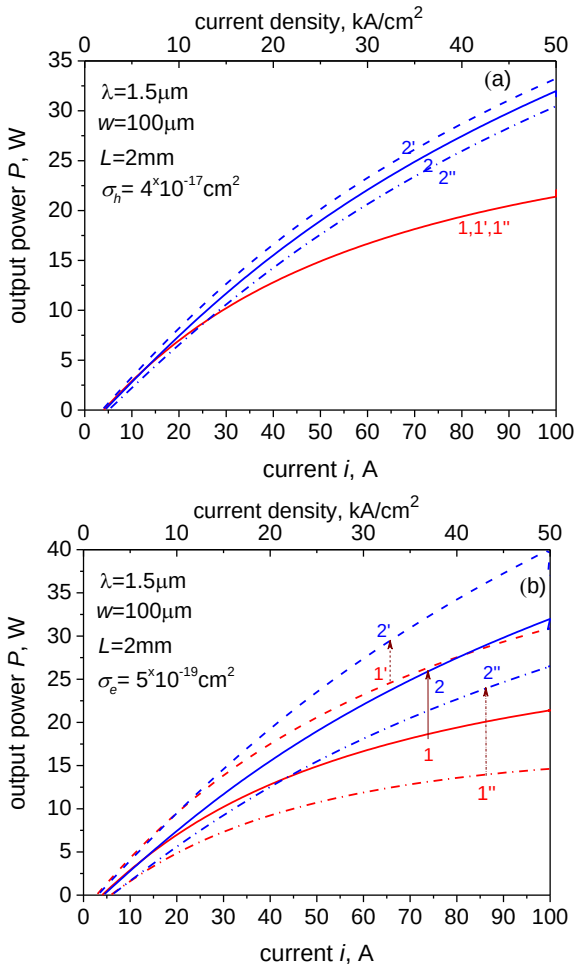

Fig. 6(a). Calculated light-current curves for low (N_D=10^{16} cm^{-3} - 1,1',1'') and high (N_D=2×10^{18} cm^{-3} - 2,2',2'') *n*-OCL doping. 1,2 – all parameters as in Table 1 (σ_e=5×10^{-19} cm^2, σ_h=4×10^{-17} cm^2); 2' - σ_e=1×10^{-19} cm^2; 2''- σ_e=1×10^{-18} cm^2. (b) As in Fig. 6(a); 1',2'- σ_h=2×10^{-17} cm^2; 1'',2''- σ_h=6×10^{-17} cm^2

The solid lines 1,2 in Figure 6 are calculated using the values of the free electron and hole absorption cross sections $\sigma_{e,h}$ as shown in Table 1. To illustrate the effects of the variation in these parameters within the limits quoted in the literature, the dashed curves 1' and 2' are calculated using the lowest value of the free electron absorption (Figure 6a) and free hole absorption (Figure 6b) cross sections quoted, and the dash-dotted curves 1'' and 2'', using the highest values. Note that the free electron absorption cross section has virtually no effect on the output power in the low-doped case, which is dominated by the free hole absorption. In general, the variation in the absorption cross-section does affect the absolute values of the power simulated. However, the beneficial effect of high doping at high power is always pronounced, particularly, as can be expected, for high values of free hole absorption cross section.

It is worth noting that the performance of the structure proposed here is predicted to compare quite favorably with the most advanced, to the best of our knowledge, devices available commercially (e.g. a device with similar cavity length, stripe width, and reflectances has demonstrated a power of about 17 W at *i*=80 A; see Fig.2 in [26]).

It has to be pointed out also that the high doping in the *n*-OCL has the additional advantage of ensuring a low voltage drop on the *n*-OCL (or, in other words, a low equivalent resistance of this layer) even at very high injection levels [12] thus allowing some additional improvement in the efficiency of laser operation. In most laser designs, it is the *p*-OCL layer that has the highest resistance in the laser structure; however if the *n*-OCL is *very* broad (several micrometers), which is often the case in asymmetric waveguide structures, reducing its resistance can offer noticeable benefit.

One may note also that structures of the kind proposed here are characterized by a large equivalent spot size (d_a/Γ_a)>>1, where d_a and Γ_a are the active layer thickness and confinement factor, respectively). This makes them very suitable, not just for the dynamically steady-state, long-pulse high power operation considered above, but also for gain switched lasers emitting optical pulses with duration ~100ps and peak powers of several tens of Watts [13],[17],[27] [28].

3. Conclusions.

To conclude, we have proposed a (semi)-analytical model for calculating the internal loss, and hence output power, in a semiconductor laser or optical amplifier structure with a highly doped *n*-OCL, including direct and indirect TPA effect as well as carrier accumulation due to current flow. The calculations presented were performed for an asymmetric waveguide structure, but the expressions derived are generic. A substantial (>40%) improvement of the output power by strong *n*-OCL doping (compared to an identical but weakly doped structure) at high pumping levels has been predicted.

It is worth noting again that the proposed method is nontrivial and somewhat counterintuitive: we propose to *reduce* the free-carrier optical absorption (at high current) by *increasing* doping in the structure, whereas previous research indicates that doping *increases* such losses by increasing the carrier density. The absorption reduction relies on the relation $\sigma_h >> \sigma_e$ (almost two orders of magnitude in our case). The reduction of losses due to FCA is then due to the fact that additional equilibrium carriers supplied by *n*-doping are only electrons, whereas nonequilibrium carriers accumulated at high currents, whose density is reduced by doping (due to the change in the dominant mechanism of transport from ambipolar diffusion to drift in the case of current-generated carriers, and due to increased recombination in the case of TPA-generated carriers), are both electrons and holes.

Acknowledgements.

This work was supported in part by the Academy of Finland (Centre of Excellence in Laser Scanning Research, contract nos. 283075 and 263705)

Appendix. The distribution of nonequilibrium carriers.

Within the OCL, the modal profile is calculated as $\psi(x)=\sqrt{\frac{2}{h_{eff}}}\cos(\kappa x-\varphi)$, where $\kappa=\frac{2\pi}{\lambda}\sqrt{n_{OCL}^2-n_0^2}$ is the transverse wave vector of the waveguide mode in the OCL, determined by the refractive index n_{OCL} of the OCL and the effective refractive index n_0 of the fundamental (TE) mode. Unlike the case of a laser with a Quantum Well active layer, in which the transverse waveguide properties of the laser are given quite accurately by a simple, semi-analytical three-layer model of [29], the bulk active layer in the design studied here affects the waveguiding noticeably. Therefore, the value of n_0, and hence the effective mode size h_{eff} and the phase shift φ, can only be, and were in our simulations, found using a numerical multilayer solver.

Eq. (4), obtained in the strong-doping condition, is linear and allows analytical solution using standard methods. Using the expression for the modal profile as above and neglecting the drift terms, the solution takes the form

$$\Delta N(x)=N_{+}\exp(x/L_D)+N_{-}\exp(-x/L_D)+$$
$$+N_{c2}\cos\left(2(\kappa x-\varphi)\right)+N_{c4}\cos\left(4(\kappa x-\varphi)\right)+\frac{3}{8}G_0\tau$$

where $L_D=\sqrt{D_h\tau}$ is the diffusion length, and the expressions of the term amplitudes are:

$$N_{c2}=\frac{G_0\tau}{2\left(1+4\kappa^2L_D^2\right)}\quad;\quad N_{c4}=\frac{G_0\tau}{8\left(1+16\kappa^2L_D^2\right)};$$
$$N_{+}=-\frac{L_DN_o^{'}\exp(-l_a/L_D)+N_{la}}{2\cosh(l_a/L_D)};$$
$$N_{-}=\frac{L_DN_o^{'}\exp(l_a/L_D)-N_{la}}{2\cosh(l_a/L_D)};$$

where $G_0=\frac{4\beta_2(x)}{\hbar\omega}\left(\frac{P}{h_{eff}w}\right)^2$ is the amplitude of the TPA generation term, and

$$N_{la}=N_{c2}\cos\left(2(\kappa l_a-\varphi)\right)+N_{c4}\cos\left(4(\kappa l_a-\varphi)\right)+\frac{3}{8}G_0\tau$$
$$N_o^{'}=2\kappa\left(2N_{c4}\sin 4\varphi+N_{c2}\sin 2\varphi\right)$$

References

[1] D. A. Veselov *et al.*, "Study of the pulse characteristics of semiconductor lasers with a broadened waveguide at low temperatures (110-120 K)," *Semiconductors*, vol. 50, no. 10, pp. 1396-1402, Oct 2016.

[2] E. A. Avrutin and B. S. Ryvkin, "The role of carrier accumulation in the optical confinement layer in output efficiency deterioration of laser diodes," in *2016 International Semiconductor Laser Conference, ISLC 2016*: Institute of Electrical and Electronics Engineers Inc., 2016, p. WS2.

[3] J. Piprek, *Semiconductor Optoelectronic Devices: Introduction to Physics and Simulation*. San Diego, CA: Academic Press, 2003.

[4] S. Krishnamurthy, Z. G. Yu, L. P. Gonzalez, and S. Guha, "Temperature- and wavelength-dependent two-photon and free-carrier absorption in GaAs, InP, GaInAs, and InAsP," *Journal of Applied Physics*, vol. 109, no. 3, Feb 2011, Art. no. 033102.

[5] G. Kyritsis and N. Zakhleniuk, "Performance of Widely Tunable MultiQuantum-Well and Bulk Laser Diodes and the Main Limiting Factors," *IEEE Journal of Quantum Electronics*, vol. 53, no. 3, 2017, Art. no. 2500216.

[6] E. A. Avrutin and B. S. Ryvkin, "Theory of direct and indirect effect of two-photon absorption on nonlinear optical losses in high power semiconductor lasers," *Semiconductor Science and Technology*, vol. 32, no. 1, Jan 2017, Art. no. 015004.

[7] B. S. Ryvkin and E. A. Avrutin, "Asymmetric, nonbroadened large optical cavity waveguide structures for high-power long-wavelength semiconductor lasers," *Journal of Applied Physics*, vol. 97, no. 12, p. 123103, Jun 2005, Art. no. 123103.

[8] N. A. Pikhtin *et al.*, "16W continuous-wave output power from 100 mu m-aperture laser with quantum well asymmetric heterostructure," *Electronics Letters*, vol. 40, no. 22, pp. 1413-1414, Oct 2004.

[9] X. Z. Wang *et al.*, "Root-Cause Analysis of Peak Power Saturation in Pulse-Pumped 1100 nm Broad Area Single Emitter Diode Lasers," (in English), *IEEE Journal of Quantum Electronics*, Article vol. 46, no. 5, pp. 658-665, May 2010.

[10] H. Wenzel, P. Crump, A. Pietrzak, X. Wang, G. Erbert, and G. Trankle, "Theoretical and experimental investigations of the limits to the maximum output power of laser diodes," *New Journal of Physics*, vol. 12, Aug 2010, Art. no. 085007.

[11] E. A. Avrutin, B. S. Ryvkin, A. S. Payusov, A. A. Serin, and N. Y. Gordeev, "Fundamental transverse mode selection and self-stabilization in large optical cavity diode lasers under high injection current densities," *Semiconductor Science and Technology*, vol. 30, no. 11, p. 115007, Nov 2015, Art. no. 115007.

[12] E. A. Avrutin and B. S. Ryvkin, "Dember type voltage and nonlinear series resistance of the optical confinement layer of a high-power diode laser," *Journal of Applied Physics*, vol. 113, no. 11, Mar 2013, Art. no. 113108.

[13] B. Ryvkin, E. A. Avrutin, and J. T. Kostamovaara, "Asymmetric-Waveguide Laser Diode for High-Power Optical Pulse Generation by Gain Switching," *Journal of Lightwave Technology*, vol. 27, no. 12, pp. 2125-2131, Jun 2009.

[14] K. H. Hasler *et al.*, "Comparative theoretical and experimental studies of two designs of high-power diode lasers," *Semiconductor Science and Technology*, vol. 29, no. 4, p. 045010, Apr 2014, Art. no. 045010.

[15] P. Crump *et al.*, "Efficient High-Power Laser Diodes," *IEEE Journal of Selected Topics in Quantum Electronics*, vol. 19, no. 4, p. 1501211, Jul-Aug 2013, Art. no. 1501211.

[16] Y. Yamagata *et al.*, "915nm high power broad area laser diodes with ultra-small optical confinement based on Asymmetric Decoupled Confinement Heterostructure (ADCH)," in *High-Power Diode Laser Technology and Applications Xiii*, vol. 9348, M. S. Zediker, Ed. (Proceedings of SPIE, 2015, p. 93480F.

[17] B. Lanz, B. S. Ryvkin, E. A. Avrutin, and J. T. Kostamovaara, "Performance improvement by a saturable absorber in gain-switched asymmetric-waveguide laser diodes," *Optics Express*, vol. 21, no. 24, pp. 29780-29791, Dec 2013.

[18] P. W. Juodawlkis *et al.*, "High-Power, Low-Noise 1.5-mu m Slab-Coupled Optical Waveguide (SCOW) Emitters: Physics, Devices, and Applications," *IEEE Journal of Selected Topics in Quantum Electronics*, vol. 17, no. 6, pp. 1698-1714, Nov-Dec 2011.

[19] P. W. Juodawlkis, J. J. Plant, J. P. Donnelly, A. Motamedi, and E. P. Ippen, "Continuous-wave two-photon absorption in a Watt-class semiconductor optical amplifier," *Optics Express*, vol. 16, no. 16, pp. 12387-12396, Aug 2008.

[20] J. Leuthold, M. Mayer, J. Eckner, G. Guekos, H. Melchior, and C. Zellweger, "Material gain of bulk 1.55 mu m InGaAsP/InP semiconductor optical amplifiers approximated by a polynomial model," *Journal of Applied Physics*, vol. 87, no. 1, pp. 618-620, Jan 2000.

[21] M. Levinshtein, S. Rumyantsev, and M. Shur, Eds. *Semiconductor Parameters: Ternary And Quaternary III-V Compounds* Singapore: World Scientific, 1996.

[22] S. M. Ryvkin, *Photoelectric Effects in Semiconductors*. New York: Consultants Bureau, 1964.

[23] G. W. Taylor and P. R. Claisse, "Transport solutions for the sch quantum-well laser-diode," *IEEE Journal of Quantum Electronics*, vol. 31, no. 12, pp. 2133-2141, Dec 1995.

[24] P. M. Smowton *et al.*, "The effect of cladding layer thickness on large optical cavity 650-nm lasers," *IEEE Journal of Quantum Electronics*, vol. 38, no. 3, pp. 285-290, Mar 2002, Art. no. Pii s0018-9197(02)01752-9.

[25] L. A. Coldren, S. W. Corzine, and M. K. Mashanovitch, *Diode Lasers and Photonic Integrated Circuits*, 2nd ed. NY: Wiley, 2012.

[26] J. F. Boucher and J. J. Callahan, "Ultra-high-intensity 1550nm single junction pulsed laser diodes," in *Laser Technology for Defense and Security Vii*, vol. 8039, M. Dubinskii and S. G. Post, Eds. (Proceedings of SPIE, 2011, pp. 80390B1-9.

[27] D. V. Kuksenkov, R. V. Roussev, S. P. Li, W. A. Wood, and C. M. Lynn, "Multiple-wavelength synthetic green laser source for speckle reduction," in *Nonlinear Frequency Generation and Conversion: Materials, Devices, and Applications X*, vol. 7917, K. L. Vodopyanov, Ed. (Proceedings of SPIE, 2011.

[28] A. Kaltenbach *et al.*, "Freely Triggerable Picosecond Pulses From a DBR Ridge Waveguide Diode Laser Near 1120 nm," *IEEE Photonics Technology Letters*, vol. 28, no. 8, pp. 915-918, Apr 2016.

[29] H. Kogelnik, "Theory of dielectric waveguides," in *Integrated Optics*, T. Tamir, Ed. Berlin – Heidelberg – New York: Springer-Verlag, 1975, pp. 15-79.